Pis'ma v ZhETF, vol. 74, iss. 1, pp. 43 – 47

Anisotropy of electronic wave functions in self-assembled InAs dots embedded in the centre of a GaAs quantum well studied by magnetotunneling spectroscopy

*E. E. Vdovin, Yu. N. Khanin, A. V. Veretennikov**, *A. Levin*+, *A. Patane*+, *Yu. V. Dubrovskii, L. Eaves*+, *P. C. Main*+, *M. Henini*+, *G. Hill*□

Institute of Microelectronics Technology RAS, 142432 Chernogolovka, Russia

+*School of Physics and Astronomy, University of Nottingham, Nottingham NG7 2RD, UK*

**Institute of Solid State Physics RAS, 142432 Chernogolovka, Russia*

□*Dept. of Electronic and Electrical Engineering, University of Sheffield, UK*

Submitted 5 June 2001

We present an experimental study of electron wavefunctions in InAs/GaAs self-assembled quantum dots by magnetotunneling spectroscopy. The electron wavefunctions have a biaxial symmetry in the growth plane, with axes corresponding to the main crystallographic directions in the growth plane. Moreover we observed the in-plane anisotropy of the subbands of the quantum well.

PACS: 71.24.+q, 73.40.Gk, 73.61.Ey, 73.61.Tm

Quantum dots (QDs) are characterised by relatively small number of electrons confined within an island with a nanometer dimension. They can confine the motion of an electron in all three spatial dimensions [1]. The strong confinement in the QD gives rise to a set of discrete and narrow electronic energy levels similar to those in atomic physics. The epitaxial growth of lattice mismatched InAs on GaAs or AlAs opens new possibilities for the simple fabrication of semiconductor nanostructures. InAs QDs are formed *in situ* during growth due to the relaxation of a strained InAs wetting layer on GaAs or AlAs [2]. The particular interest lies in their uniformity and small size: a lateral dimension 10–20 nm and height 3–4 nm. Several theoretical approaches have been used to calculate the eigenstates of InAs QDs [3]. The results of the calculation depend strongly on the assumed shape and composition of the QDs. Experimentally, the quantized energy levels of a given potential can be probed using various spectroscopic techniques. The corresponding wave functions are much more difficult to measure. Information about the extent of the carrier wavefunction for the ground state of a QD was obtained from tunneling measurements in a magnetic field [4]. Also, the anisotropy of electronic wave function in self-aligned InAs QDs was deduced from magnetic-field-dependent photoluminescence spectroscopy [5]. However, until recently there have been no reported measurements of the detailed spatial form of the wavefunctions of the ground and excited states of the QD. Recently, it has been demonstrated that magnetotunneling spectroscopy can be employed as nonivasive probe to produce images of the probability density of the electron confined in a QD [6]. In this work, we use magnetotunneling spectroscopy to investigate in detail of the spatial form of the wave function of the electron states of a double-barrier resonant tunnelling diode with InAs QDs embedded in the centre of a GaAs quantum well (the ground and excited states of the QDs and confined subbunds of the quantum well). We measure the dependence of the resonant tunnelling current through the QD states as a function of magnetic field, B, applied perpendicular to the tunnelling direction. This allows us to map out the full spatial form of the probability density of the ground and excited states of the QDs and confined subbunds of the quantum well. The electron wavefunctions have a biaxial symmetry in the growth plane, with axes corresponding quite closely (within measurement error of 15°) to the main crystallographic directions $X - [01\bar{1}]$ and $Y - [\bar{2}33]$ for $(311)B$ substrate orientation. For a similar InAs QD structure grown on a (100)-substrate we also obtained characteristic probability density maps of ground and exited states. Moreover we observed the in-plane anisotropy of the subbands of the quantum well.

The InAs QDs are embedded in a $n{-}i{-}n$, resonant tunnelling diode. The samples were grown by molecular beam epitaxy on a GaAs substrate with the orientations (100) and $(311)B$. A layer of InAs QDs, nominally 2.3 monolayer thick, was placed in the cen-

tre of a 9.6 nm wide GaAs quantum well (QW) with 8.3 nm $Al_{0.4}Ga_{0.6}As$ confining barriers, sandwiched between two nominally-undoped 50 nm GaAs spacer layers. The intrinsic region is surrounded by graded n-type contact layers, with the doping concentration increasing from $2 \cdot 10^{17}\,cm^3$ to $3 \cdot 10^{18}\,cm^{-3}$. The layers were grown at 600 °C, and there was a growth interrupt before the QDs were grown at 480 °C. For comparison, we also studied two control samples grown with the same sequence of layers, except one has only a thin InAs two-dimensional wetting layer (i.e. containing no QDs) and the other has no InAs layer at all. The samples were processed into circular mesa structures of diameters between 50 μm and 200 μm, with ohmic contacts to the doped regions.

Fig.1 shows a schematic energy band diagram for our device under bias voltage. X and Y define the two

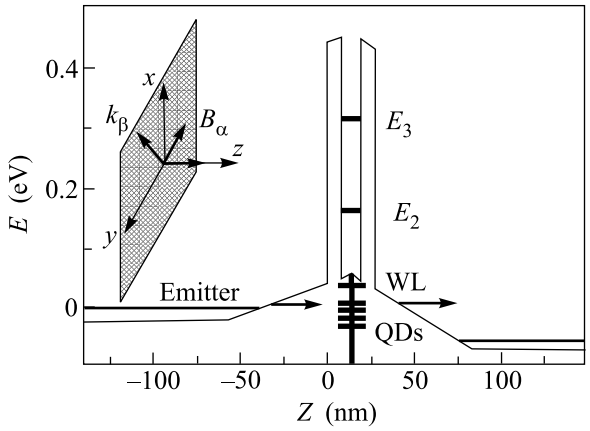

Fig.1. Schematic conduction band profile under an applied bias of an n–i–n GaAs/(AlGa)As double barrier resonant tunneling diode incorporating InAs QDs. Inset: Orientation of the magnetic field, B, and current, I, in the magnetotunnelling experiment. X and Y define the two main crystallographic axis, $[01\bar{1}]$ and $[\bar{2}33]$, respectively, in the (311)-oriented GaAs substrate. α and β indicate, respectively, the direction of B and of the momentum acquired by the tunnelling electron due to the action of the Lorentz force

main crystallographic axis in the plane perpendicular to growth direction, Z (see inset). The layer of InAs QDs introduces a set of discrete electronic states below the GaAs conduction band edge. At zero bias voltage, equilibrium is established by electrons diffusing from the doped GaAs layers and filling some dot states. The resulting negative charge in the QW produces depletion layers in the regions beyond the (AlGa)As barriers. By applying a bias voltage to the emitter layer, V, the QD energy level is shifted in energy with respect to both contacts. When a particular dot state is resonant with an adjacent filled state in the biased electron emitter layer, electrons tunnel through the dot into the collector and a current flows as shown schematically in Fig.1. Therefore, as we adjust the voltage we can study different energy states of the QDs. At sufficiently high voltages we are able to observe two separate resonances in the current related to confined subbands of the QW states.

Fig.2 shows a typical low-temperature (T = 1.2 K) $I(V)$ curve. The device contains InAs QDs grown on

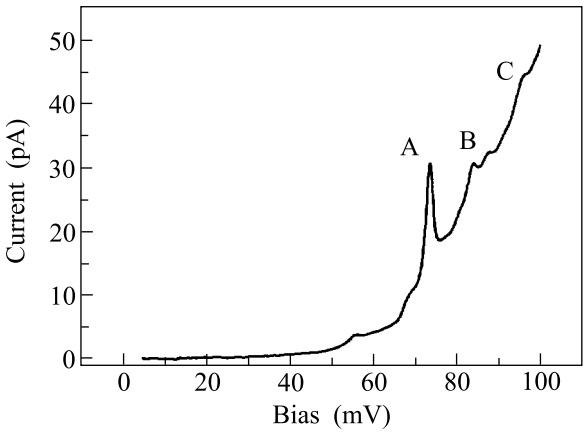

Fig.2. Low-temperature (T = 1.2 K) current-voltage characteristics, $I(V)$. Dots are grown on (311)B substrate orientation

a (311)B-oriented GaAs substrate. Similar were obtained for QDs grown on a (100)-substrate. We observe a series of resonant peaks corresponding to carrier tunnelling into the dot states. Pronounced current features appear at biases as low bias as 55 mV. They are superimposed on a rising background current and cannot be resolved for $V > 200$ mV. These features are not observed in our control samples which do not contain QDs and are thereforewe can ascribe them to the InAs QD layer. Despite the large number of quantum dots in our sample (10^6–10^7 for a 100 μm diameter mesa), we observed only a small number of resonant peaks over the bias range ($\sim$ 200 mV) close to the threshold for current flow. This behaviour has been reported in earlier studies [4, 6–12] and, although not fully understood, is probably related to the limited number of conducting channels in the emitter that can transmit electrons from the doping layer to the quantum dots at low bias. There is no reason to believe that the dots studied are atypical of the distribution as a whole. On increasing the temperature to 4.2 K, the main peaks are still prominent, but much weaker features, which may be related to density-of-state fluctuation in the emitter [13], are strongly suppressed. A key observation is that many peaks look similar so we cannot tell if the peaks are due to tunneling through the

states of a single dot or several dots. In the following, we will concentrate on three voltage regions labelled A, B and C. We will focus on the magnetic field dependence of the QD resonances and on how this provides detailed information about the form of the wavefunction associated with an electron in the QD state.

Fig.3a shows the low-temperature ($T = 4.2$ K) $I(V)$ characteristics in the presence of a magnetic field, B.

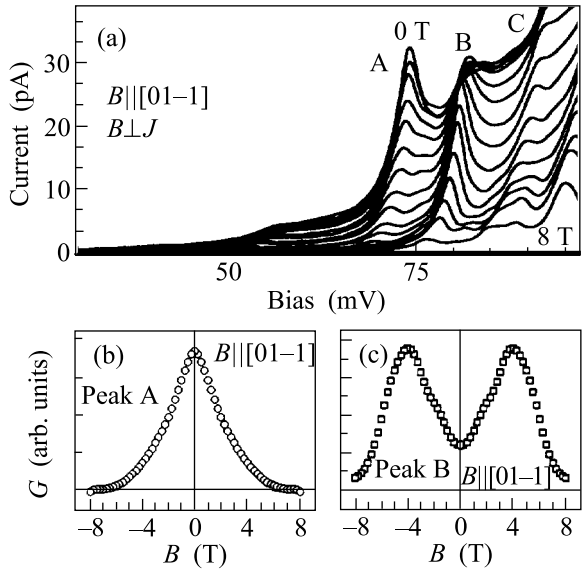

Fig.3. (a) Low-temperature ($T = 4.2$ K) $I(V)$ characteristics in the presence of a magnetic field, B. The direction of B is perpendicular to the current flow. (b) and (c) Dependence of conductance, G, on magnetic field for B parallel to $[01\bar{1}]$ for different QDs states. B was varied from 0 to 8 T with the step of 0.5 T

The direction of B is perpendicular to the current flow and lies in the (X, Y) plane (see Fig.1). The axis $[01\bar{1}]$ and $[\bar{2}33]$ define the two main crystallographic axis in the plane perpendicular to growth direction [311]. The amplitude of each resonance exhibits a strong dependence on the intensity of B. In particular, with increasing B, the low-voltage resonances "A" decrease steadily in amplitude, whereas the others, "B" and "C", have a non-monotonic magnetic field dependence. The Fig.3b and 3c show clearly two characteristic types of magnetic field dependence: type "A" shows a maximum on $G(B)$ at $B = 0$ T followed by a steady decay to zero at around 8 T; type "B" shows a broad maximum at ~ 4.5 T, followed by a gradual decay to zero.

Fig.4a shows the $I(V)$ characteristics in an in-plane magnetic field of 4.5 T. The first curve (circles) is for $B\|[01\bar{1}]$; the second curve (triangles) is for $B\|[\bar{2}33]$. We observe a clear anisotropy in the dependence of $I(V)$ on B for the two field orientations. As can be clearly seen

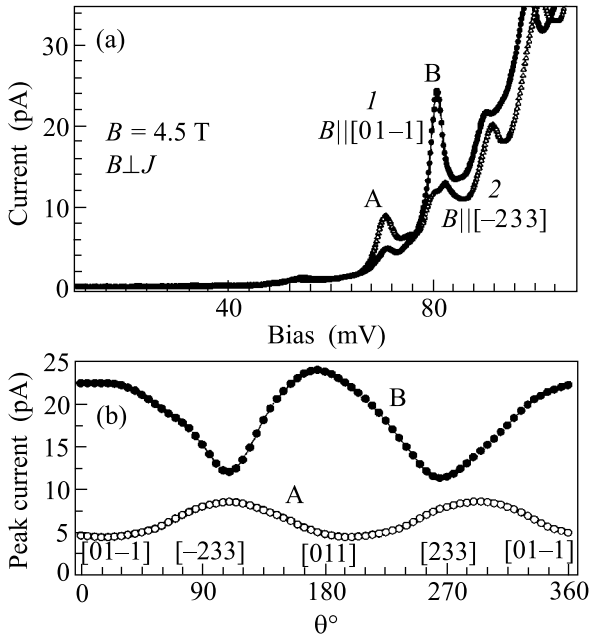

Fig.4. (a) $I(V)$ characteristics in an in-plane magnetic field of 4.5 T. The first curve (circles) is for $B\|[01\bar{1}]$; the second curve (triangles) is for $B\|[\bar{2}33]$; (b) angular dependence of the peaks current

in Fig.4a peaks "A" and "B" in the $I(V)$ plot reveal a strong anisotropy of about $\rho \sim 0.5$. We have also determined angular dependence of the peaks. The results are plotted in Fig.4b for peaks "A" and "B". Note that all peaks, observed over the bias range (~200 mV) have a maxima in current amplitude at orientation of a field $B\|[01\bar{1}]$ or $B\|[\bar{2}33]$. The main effect to be noted from Fig.4 is the dependence of the current as a function of the in-plane magnetic field orientation.

Fig.5a shows the $I(V)$ characteristics in an in-plane magnetic field of 4.5 T in the voltage range corresponded to the resonant tunneling through the second subband of the quantum well. The first curve (circles) is for $B\|[01\bar{1}]$; the second curve (triangles) is for $B\|[\bar{2}33]$. The anisotropy of the observed resonance is plotted in Fig.5b. The angular dependence of the peak current measured with magnetotunneling spectroscopy is interpretated as a direct representation of the in-plane anisotropy of a subband [14 – 16]. The anisotropy of the quantum well subband can be induced by the orientation of the Al–As bonds at neighbouring interfaces of the quantum well [15].

We can understand the magnetic field dependence of the features in terms of the effect of B on a tunnelling electron. Let α, β, and Z indicate, respectively, the direction of B, the direction normal to B in the growth plane (X, Y), and the normal to the tunnel barrier, re-

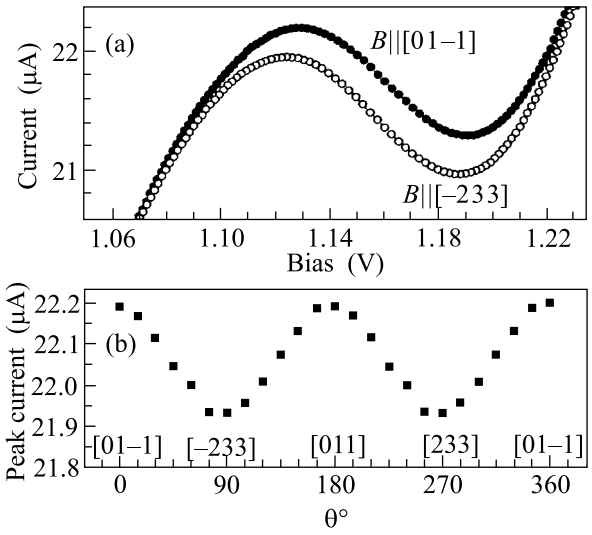

Fig.5. (a) $I(V)$ characteristics in an in-plain magnetic field of 4.5 T in the voltage range corresponded to the resonant tunneling through the second subband of the quantum well. The first curve (solid circles) is for $B\|[01\bar{1}]$; the second curve (open circles) is for $B\|[\bar{2}33]$; (b) angular dependence of the peak current

spectively (see Fig.1b). When an electron tunnels from the emitter into the dot, it acquires an additional in-plane momentum given by [17]

$$k_\beta = eB\Delta s/\hbar \qquad (1)$$

where Δs is the effective distance tunnelled along Z. This effect can be understood semiclassically in terms of the increased momentum along β, which is acquired by the tunnelling electron due to the action of the Lorentz force. In terms of mapping out the spatial form of an electronic state, we can envisage the effect of this shift in as analogous to that of the displacement, in real space, of the atomic tip in a STM imaging measurement. The applied voltage allows us to tune resonantly to the energy of a particular QD state. Then, by measuring the variation of the tunnel current with B, we can determine the size of the matrix element that governs the quantum transition of an electron as it tunnels from a state in the emitter layer into a QD. In our experiment, the tunnelling matrix element is most conveniently expressed in terms of the Fourier transforms $\Phi_{i,f}(\underline{k})$ of the conventional real space wavefunctions [17, 18]. Here the subscripts i and f indicate the initial (emitter) and final (QD) states of the tunnel transition. Relative to the strong spatial confinement in the QD, the initial emitter state has only weak spatial confinement. Hence, in $\underline{k}$-space corresponds to a sharply peaked function with a finite value only close to $\underline{k} = 0$. Since the tunnel current is given by the square of the matrix element involving $\Phi_i(\underline{k})$ and $\Phi_{QD}(\underline{k})$, the narrow spread of $\underline{k}$ for $\Phi_i(\underline{k})$ allows us to determine the form of $\Phi_{QD}(\underline{k})$ by varying B and hence $\underline{k}$ according to (1). Thus by plotting $G(B)$ for a *particular* direction of B we can measure the dependence of $|\Phi_{QD}(\underline{k})|^2$ along the $\underline{k}$-direction perpendicular to B. Then, by rotating B in the plane (X, Y) and making a series of measurements of $I(B)$ with B set at regular intervals ($\Delta\theta \sim 5^\circ$) of the rotation angle θ, we obtain a full spatial profile of $|\Phi_{QD}(k_X, k_Y)|^2$. This represents the projection in $\underline{k}$-space of the probability density of a given electronic state confined in the QD.

The model provides a simple explanation of the magnetic field dependence of the resonant current features "A–C". In particular, the *forbidden* nature of the tunnelling transition associated with "B" at $B = 0$ T is due to the odd parity of the final state wavefunction, which corresponds to the first excited state of a QD. The applied magnetic field (i.e. the Lorentz force) effectively breaks the mirror symmetry at $B = 0$ and thus makes the transition *allowed*.

Fig.6 shows the spatial form of $G(B) \sim |\Phi_{QD}(k_X, k_Y)|^2$, in the plane (k_X, k_Y) for the two representative QD states corresponding to the

Fig.6. Distribution in the plane (k_X, k_Y) of the differential conductance, $G = dI/dV$, for three representative states. This provides a spatial map of $|\Phi_{QD}(k_X, k_Y)|^2$, the square of the Fourier transform, $\Phi_{QD}(k_X, k_Y)$, of the probability density of the electron confined in the dot. X and Y define the two main crystallographic axis, $[01\bar{1}]$ and $[\bar{2}33]$, respectively, in the (311)-oriented GaAs plane

labelled features in Fig.3b and 3c. The $\underline{k}$-values are estimated from relation (1), assuming Δs has nominal value of 30 nm which we estimate from capacitance measurements and from the doping profile and composition of the device. The contour plots reveal clearly the characteristic form of the probability density distribution of a ground state orbital and the characteristic lobes of the higher energy states of the QD. The electron

wavefunctions have a biaxial symmetry in the growth plane, with axes corresponding quite closely (within measurement error of 15°) to the main crystallographic directions $X - [01\bar{1}]$ and $Y - [\bar{2}33]$ for $(311)B$-substrate orientation. For a similar InAs QD structure grown on a (100)-substrate we also obtained characteristic probability density maps of ground and exited states.

To summarise, we have observed features in $I(V)$ corresponding to resonant tunnelling through a limited number of discrete states whose wavefunctions display the symmetry of the ground state and excited states of quantum dots. With the simple device configuration we have used, it is not possible to tell whether an excited state feature and a ground state feature correspond to the same quantum dot. This question could be resolved by new experiments on structures with electrostatic gates.

In conclusion, we have shown how the magnetotunnelling spectroscopy provides a new means of probing the spatial form of the wavefunctions of electrons confined in quantum dots and quantum well. The study revealed a biaxial symmetry of QD states in the growth plane. We observed the elliptical shape of the ground state and the characteristic lobes of the higher energy states. Moreover we observed the elliptical shape of the subbands of the quantum well.

The work is partly supported by RFBR (# 00-02-17903), INTAS-RFBR(# 95-849) and EPSRC (UK). AL gratefully acknowledges the support of the FAPESP Foundation (Brazil). EEV gratefully acknowledge supports from the Royal Society. We are gratefully to V. A. Tulin and V. G. Lysenko for helpful discussions and V. V. Belov and A. Orlov for technical assistance.

1. D. Bimberg, M. Grundmann, and N. N. Ledentsov, Quantum Dot Heterostructures, John Wiley & Sons, New York, 1999.
2. C. Pryor, Phys. Rev. **B57**, 7190 (1998); L.-W. Wang, J. Kim, and A. Zunger, Phys. Rev. **B59**, 5678 (1999); O. Stier, M. Grundmann, and D. Bimberg, Phys. Rev. **B59**, 5688 (1999); W. Yang, H. Lee, T. J. Jonhson et al., Phys. Rev. **B61**, 2784 (2000).
3. M. F. Crommie, C. P. Lutz, and D. M. Eigler, Nature **262**, 218 (1993).
4. M. Narihiro, G. Yusa, Y. Nakamura et al., Appl. Phys. Lett. **70**, 105 (1997).
5. H. J. Zhu, M. Ramsteiner, K. H. Ploog et al., Phys. Rev. **B62**, 16314 (2000).
6. E. E. Vdovin, A. Levin, A. Patane et al., Science **290**, 122 (2000).
7. A. Patane, A. Polimeni, L. Eaves et al., Phys. Rev. **B62**, 13595 (2000).
8. P. C. Main, A. S. G. Tornton, R. J. A. Hill et al., Phys. Rev. Lett. **84**, 729 (2000).
9. T. Suzuki, K. Nomoto, K. Taira, and I. Hase, Jpn. J. Appl. Phys. Part 1 **36**, 1917 (1997).
10. I. E. Itskevich, T. Ihn, A. Thornton et al., Phys. Rev. **B54**, 16401 (1996).
11. I. Hapke-Wurst, U. Zeitler, H. Frahm et al., Phys. Rev. **B62**, 12621 (2000).
12. D. G. Austing, S. Tarucha, P. C. Main et al., Appl. Phys. Lett. **75**, 671 (1999).
13. T. Schmidt, R. J. Haug, V. I. Fal'ko et al., Phys. Rev. Lett. **78**, 1541 (1997).
14. F. Aristone, J. F. Palmier, P. Gassot et al., Appl. Phys. Lett. **67**, 2916 (1995).
15. P. W. Lukey, J. Caro, T. Zijlstra et al., Phys. Rev. **B57**, 7132 (1998).
16. T. Reker, H. Im, L. E. Bremme et al., *Proc. of Intern. Conf. on Semiconductor Physics*, ICPS 25 International Conference on Semiconductor Physics, ICPS25, Osaka, Japan, 2000.
17. P. H. Beton, H. Buhmann, L. Eaves et al., Phys. Rev. Lett. **75**, 1996 (1995).
18. J .W. Sakai, T. M. Fromhold, P. H. Betton et al., Phys. Rev. **B48**, 5664 (1993).